

# Control of Monolayer Assembly Structure by Hydrogen Bonding Rather Than by Adsorbate–Substrate Templating

Robert S. Clegg and James E. Hutchison\*

Contribution from the Department of Chemistry and Materials Science Institute, University of Oregon, Eugene, Oregon 97403-1253

Received January 11, 1999

**Abstract:** Stratified amide-containing self-assembled monolayers (SAMs) provide opportunities for investigating the fundamental dependence of supramolecular structure upon molecular constitution. We report a series of amide-containing alkanethiol SAMs ( $C_n$ -1AT/Au,  $n = 9, 11-16, 18$ ) in which the hydrophobic overlayer thickness is systematically varied and the thickness of the polar region is held constant. The results from X-ray photoelectron spectroscopy, contact angle goniometry, reflective IR spectroscopy, and electrochemical measurements provide a consistent structural picture of the series. The amide underlayers in all the SAMs are well-ordered and extensively hydrogen bonded. However, the alkyl chains are disordered below  $n = 15$ . Comparison of the assembly structures shows that the chain length threshold for alkyl ordering is several methylenes higher than in  $n$ -alkanethiol SAMs. This indicates that alkyl chains adjacent to an amide underlayer are destabilized as compared to  $n$ -alkanethiols and that the amide underlayer destructively interferes with alkyl close packing as compared to the Au(111)–sulfur template. However, the amide regions of the SAMs are all well-ordered, showing that the amide sublayer acts as a “template” that is independent of alkyl chain length. The amide region dominates over gold–sulfur epitaxy in establishing the structure of these assemblies, and the amide–alkyl boundary provides an example of a “rigid–elastic” buried organic interface. Implications of these studies for molecular control of bulk properties, lipid-linked protein structure and function, buried organic interfaces in other systems, rationally designed ordered multilayers, and hybrid supramolecular systems are discussed.

## Introduction

Self-assembly of ultrathin organic films has found widespread use in the control of surface properties as well as the fundamental study of interfacial phenomena. The formation,<sup>1a–c</sup> structure,<sup>1c–f</sup> properties,<sup>1f–h</sup> and applications<sup>2</sup> of self-assembled monolayers (SAMs) of  $n$ -alkanethiols on gold and other coinage metals has been thoroughly reviewed. Although lithographic patterning of surface bound films has received much attention,<sup>2e,f</sup> vertical differentiation with controlled incorporation of sublayered architectures at the molecular level is relatively unstudied. Vertical structuring is desired for applications of SAMs for nonlinear optics,<sup>3a</sup> electron-transfer catalysis,<sup>3b</sup> protein<sup>3c</sup> and cell<sup>3d</sup> immobilization, physical<sup>3c</sup> and chemical<sup>3f</sup> sensing, artificial photosynthesis,<sup>3g</sup> electron-transfer studies,<sup>3h</sup> biocompatible surfaces,<sup>3i</sup> and corrosion passivation.<sup>3j</sup> The greatest complexity

in vertically architected films has been achieved by sequential multilayer growth.<sup>4</sup> However, Ulman proposed in 1990 that *monolayer* films might be similarly tiered to form vertical domains with contrasting dielectric or optical properties.<sup>5</sup> Such films are desirable because the adsorption process is one-step and monolayers tend to be better ordered than multilayers.<sup>6</sup> The introduction of functional groups in alkanethiol SAMs offers ready access to such stratification. Thus far, well-ordered, internally stratified alkanethiol-based SAMs are limited to those in which diynes, ethers, and appropriately placed sulfones and amides are incorporated in the hydrocarbon backbones of the precursors.<sup>7,8</sup> Often, internal functionalities result in decreased

(3) For reviews of the application of SAMs in these areas of interest, see: (a) Nie, W. *Adv. Mater.* **1993**, *5*, 520–545. (b) Offord, D. A.; Sachs, S. B.; Ennis, M. S.; Eberspacher, T. A.; Griffin, J. H.; Chidsey, C. E. D.; Collman, J. P. *J. Am. Chem. Soc.* **1998**, *120*, 4478–4487. (c) Madoz, J.; Kuznetsov, B. A.; Medrano, F. J.; Garcia, J. L.; Fernandez, V. M. *J. Am. Chem. Soc.* **1997**, *119*, 1043–1051. (d) Mrksich, M. *Cell. Mol. Life Sci.* **1998**, *54*, 653–662. (e) Pope, J. M.; Tan, Z.; Kimbrell, S.; Buttry, D. A. *J. Am. Chem. Soc.* **1992**, *114*, 10085–10086. (f) Li, S.; Crooks, R. M. *Langmuir* **1993**, *9*, 1775–1780. (g) Hiroshi, I.; Hirokyuki, N.; Shinichiro, O.; Kiminori, U.; Hiroko, Y.; Takayuki, A.; Koichi, T.; Yoshiteru, S. *Langmuir* **1998**, *14*, 5335–5338. (h) Yu, H.-Z.; Zhang, H.-L.; Liu, Z.-F. *Langmuir* **1998**, *14*, 619–624. (i) Miura, Y.; Kimura, S. *Langmuir* **1998**, *14*, 2761–2767. (j) Zamborini, F. P.; Crooks, R. M. *Langmuir* **1998**, *14*, 3279–3286.

(4) For a review, see: Mallouk, T. E.; Kim, H.-N.; Ollivier, P. J.; Keller, S. W. In *Comprehensive Supramolecular Chemistry*, Vol. 7; Alberti, G., Bein, T., Eds.; Elsevier: Oxford, U.K., 1996; pp 189–217.

(5) Kuhn, H.; Ulman, A. In *Thin Films, Vol. 20; Organic Thin Films and Surfaces: Directions for the Nineties*; Ulman, A., Ed.; Academic: San Diego, CA, 1995; pp 1–10.

(6) Laibinis, P. E.; Palmer, B. J.; Lee, S.-W.; Jennings, G. K. *Thin Films* **1998**, *24*, 1–41.

(1) (a) Poirier, B. E.; Pylant, E. D. *Science* **1996**, *272*, 1145–1148. (b) Karpovich, D. S.; Schessler, H. M.; Blanchard, G. J. *Thin Films* **1998**, *24*, 44–81. (c) Ulman, A. *Chem. Rev.* **1996**, *96*, 1533–1554. (d) Liu, G.-y.; Xu, S.; Cruchon-Dupeyrat, S. *Thin Films* **1998**, *24*, 82–111. (e) Fenter, P. *Thin Films* **1998**, *24*, 112–149. (f) Dubois, L. H.; Nuzzo, R. G. *Annu. Rev. Phys. Chem.* **1992**, *43*, 437–463. (g) Finklea, H. O. In *Electroanalytical Chemistry: A Series of Advances*; Bard, A. J., Ed.; Dekker: New York, 1996; pp 110–336. (h) Delamarche, E.; Michel, B.; Biebuyck, H. A.; Gerber, C. *Adv. Mater.* **1996**, *8*, 719–729.

(2) (a) Murray, R. W.; Ewing, A. G.; Durst, R. A. *Anal. Chem.* **1987**, *59*, 379A–385A. (b) Mrksich, M.; Whitesides, G. M. *Annu. Rev. Biophys. Biomol. Struct.* **1996**, *25*, 55–78. (c) Crooks, R. M.; Ricco, A. J. *Acc. Chem. Res.* **1998**, *31*, 219–227. (d) Liu, J.; Kim, A. Y.; Wang, L. Q.; Palmer, B. J.; Chen, Y. L.; Bruinsma, P.; Bunker, B. C.; Exarhos, G. J.; Graff, G. L.; Rieke, P. C.; Fryxell, G. E.; Virden, J. W.; Tarasevich, B. J.; Chick, L. A. *Adv. Colloid Interface Sci.* **1996**, *69*, 131–180. (e) Xia, Y.; Whitesides, G. M. *Angew. Chem., Int. Ed. Engl.* **1998**, *37*, 550–575. (f) Tien, J.; Younan, X.; Whitesides, G. M. *Thin Films* **1998**, *24*, 227–254.

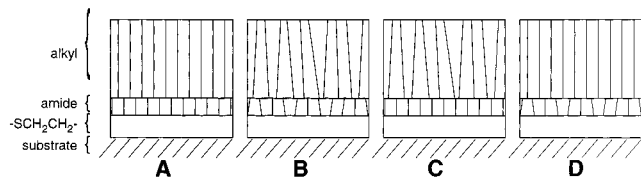


**Figure 1.** Possible assembly structures of hybrid amide-alkyl SAMs in which amide regions are sandwiched between a gold substrate and an alkyl region. The parallel and nonparallel lines indicate ordered and disordered regions respectively and do not contain information about chain orientations. (A) Fully ordered SAM. (B) Fully disordered SAM. (C) Disordered alkyl overlayer with an ordered amide underlayer. (D) Ordered alkyl overlayer with a disordered amide underlayer.

order, as with alkenes and alkynes, N- and C-substituted diglycines, single amide groups, and sulfones.<sup>8–11</sup> Obviously, disorder is incompatible with well-defined stratification and stability of lateral patterning.<sup>5,12</sup> Systematic studies of the effect of sublayers of contrasting polarizability upon SAM order and structure have not been reported.

Our approach toward a well-defined vertical architecture involves replacing methylene units of alkanethiol SAMs with amide groups. Previously, amide groups have been incorporated at various levels in monolayers for a number of reasons. Primary amides have been used as platforms for biomolecule immobilization and cell adhesion.<sup>2b</sup> Internal (secondary and tertiary) amides, in addition to providing efficient synthetic routes,<sup>10</sup> have been incorporated with the goals of controlling molecular orientation<sup>11</sup> and improving SAM stability.<sup>9,12</sup> We previously reported well-ordered, extensively hydrogen bonded SAMs containing one<sup>7a</sup> and three<sup>9a</sup> internal amide groups. As ordered, stratified SAMs, these systems have great potential for studying the relationship between molecular and supramolecular structure<sup>9,13</sup> and the nature of buried interfaces *within* organic assemblies.<sup>13</sup> In addition, amide-based stratified films may prove advantageous for lithographic applications because hydrogen bonding interactions should promote monolayer stability<sup>9a</sup> and hinder adsorbate diffusion across domain boundaries in mixed SAMs.<sup>5,12</sup>

The rational design of ordered, stratified, amide-containing SAMs requires an understanding of how the various material sublayers affect each other. In these monolayers, two adjacent regions are immediately obvious: (1) the more polar amide underlayer lying proximal to the substrate and (2) the overlying hydrophobic alkyl layer. The interactions within and between these two sublayers will dictate the overall assembly structure and order. Several scenarios are possible: the film may be fully ordered (Figure 1A), completely disordered (Figure 1B), or only partially ordered (Figure 1C,D).

(7) (a) Clegg, R. S.; Hutchison, J. E. *Langmuir* **1996**, *12*, 5239–5243. (b) Batchelder, D. N.; Evans, S. D.; Freeman, T. L.; Häußling, L.; Ringsdorf, H.; Wolf, H. *J. Am. Chem. Soc.* **1994**, *116*, 1050–1053.

(8) (a) Sinniah, K.; Cheng, J.; Terrettaz, S.; Reutt-Robey, J. E.; Miller, C. J. *J. Phys. Chem.* **1995**, *99*, 14500–14505. (b) Evans, S. D.; Goppert-Berarducci, K. E.; Urankar, E.; Gerenser, L. J.; Ulman, A. *Langmuir* **1991**, *7*, 2700–2709.

(9) (a) Clegg, R. S.; Reed, S. M.; Hutchison, J. E. *J. Am. Chem. Soc.* **1998**, *120*, 2486–2487. (b) Tam-Chang, S.-W.; Biebuyck, H. A.; Whitesides, G. A.; Jeon, N.; Nuzzo, R. A. *Langmuir* **1995**, *11*, 4371–4382.

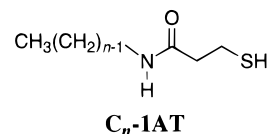
(10) Chechik, V.; Schönherr, H.; Vancso, G. J.; Stürling, C. J. M. *Langmuir* **1998**, *14*, 3003–3010.

(11) Zhang, J.; Zhang, H. L.; Chen, M.; Zhao, J.; Liu, Z. F.; Li, H. L. *Ber. Bunsen-Ges. Phys. Chem.* **1998**, *102*, 701–703.

(12) Lenk, T. J.; Hallmark, V. M.; Hoffman, C. L.; Rabolt, J. F.; Castner, D. G.; Erdelen, C.; Ringsdorf, H. *Langmuir* **1994**, *10*, 4610–4617.

(13) Clegg, R. S.; Reed, S. M.; Smith, R. K.; Barron, Bridgette L.; Rear, J. A.; Hutchison, J. E. Submitted for publication.

By systematically varying the hydrophobic overlayer thickness while holding constant the thickness of the polar amide region, we show how the interaction of these two sublayers influences the order of the entire assembly. The structural interpretation based on an array of analytical data for a series of alkanethiol SAMs containing a single, deeply buried amide group ( $C_n$ -1AT/Au;  $n = 9, 11–16, 18$ ) is presented. For  $n \geq$



15, the films are fully ordered (Figure 1A), but those with shorter alkyl “tails” show selective disorder of the hydrocarbon region (Figure 1C). In the *n*-alkanethiol series, an analogous chain length ordering threshold of  $n = 10$  has been attributed to the summation of hydrophobic interactions.<sup>14</sup> The observed trends among the assembly structures lead to two new concepts: (1) alkyl chain packing adjacent to an amide underlayer is destabilized as compared to *n*-alkanethiols, yet very highly ordered assemblies are formed above a characteristic threshold chain length, and (2) the buried organic interface in one-amide assemblies behaves in a “rigid-elastic” manner, with the rigid amide underlayer templating the alkyl chains analogously to the current understanding of *n*-alkanethiols on gold.

## Experimental Section

**Materials and Synthesis.** Dichloromethane was distilled from calcium hydride immediately before use. All other solvents and reagents were used as received from Aldrich, Bachem, Fluka, or Lancaster as previously described.<sup>7a,9a</sup>

As a representative procedure, the synthesis of 3-mercapto-*N*-nonylpropionamide  $C_9$ -1AT is described here. In a 250 mL round-bottom flask fitted with a magnetic stir bar, 0.5518 g (3.730 mmol) of *S*-acetyl-3-mercaptopropionic acid,<sup>7a,18</sup> 0.7011 g (3.694 mmol) of 3-*N*-dimethylaminopropyl-*N*-ethylcarbodiimide,<sup>19</sup> and 0.0447 g (0.369 mmol) of 4-(dimethylamino)pyridine were dissolved in 100 mL of dichloromethane at room temperature. Upon addition of 0.670 mL (3.66 mmol) of *n*-nonylamine, the solution remained clear and colorless but cooled transiently. After being stirred under nitrogen for 2–4 h, the organic solution was washed with  $3 \times 100$  mL of saturated sodium bicarbonate,  $3 \times 100$  mL of 0.01 M hydrochloric acid (adding 25 mL of brine as needed to resolve emulsions), and  $1 \times 100$  mL of distilled water. The organic portion was separated, dried over sodium sulfate, and filtered. The solvent was removed in vacuo to yield a white solid. In an Erlenmeyer flask, 1.24 g of sodium hydroxide was dissolved in 125 mL of absolute methanol. This was added all at once to the white solid in a 250 mL round-bottom flask. After being stirred under nitrogen for 0.5–1 h, 40 mL of 5% hydrochloric acid was added all at once.<sup>7a,9b</sup> A white precipitate immediately formed, and stirring was continued for 0.5 h. After addition of 25–50 mL of brine, the product was extracted with  $3 \times 80$  mL of dichloromethane. The organic portion was washed with  $3 \times 100$  mL of distilled water (adding 25 mL of brine as needed to resolve emulsions), dried over sodium sulfate, and filtered. The solvent was removed in vacuo to yield a white micro-

(14) (a) Bain, C. D.; Troughton, E. B.; Tao, Y.-T.; Evall, J.; Whitesides, G. M.; Nuzzo, R. G. *J. Am. Chem. Soc.* **1989**, *111*, 321–335. (b) Porter, M. D.; Bright, T. B.; Allara, D. L.; Chidsey, C. E. D. *J. Am. Chem. Soc.* **1987**, *109*, 3559–3568.

(15) Dettre, R. H.; Johnson, R. E. *J. Phys. Chem.* **1965**, *69*, 1507–1515.

(16) Bar, G.; Rubin, S.; Cutts, R. W.; Taylor, T. N.; Zawadowski, T. A., Jr. *Langmuir* **1996**, *12*, 1172–1179.

(17) Finklea, H. O.; Hanshew, D. D. *J. Electroanal. Chem.* **1993**, *347*, 327–340.

(18) Daeniker, H. U.; Druery, J. *Helv. Chim. Acta* **1957**, *40*, 2148–2156.

(19) (a) Bodanszky, M. *Principles of Peptide Synthesis*; Springer-Verlag: New York, 1984; pp 9–58. (b) Sheehan, J. C.; Cruickshank, P. A.; Boshart, G. I. *J. Org. Chem.* **1961**, *26*, 2525–2528.

crystalline solid which was recrystallized from 95% ethanol. Yield (with respect to *n*-alkylamine starting material): 87%. Mp: 45.6–47.5 °C. <sup>1</sup>H NMR (300 MHz, CDCl<sub>3</sub>): δ 5.71 (broad, 1H), 3.26 (m, 2H), 2.82 (m, 2H), 2.47 (t, *J* = 6.8 Hz, 2H), 1.62 (t, *J* = 8.4 Hz, 1H), 1.49 (m, 2H), 1.45–1.24 (broad overlapping resonance, 12H), 0.88 (t, *J* = 6.6 Hz, 3H).

3-Mercapto-*N*-*n*-undecylpropionamide C<sub>11</sub>-1AT was synthesized analogously to C<sub>9</sub>-1AT with the substitution of *n*-undecylamine for *n*-nonylamine. Yield: 85%. Mp: 57.5–59.0 °C. <sup>1</sup>H NMR (300 MHz, CDCl<sub>3</sub>): δ 5.55 (broad, 1H), 3.26 (m, 2H), 2.82 (m, 2H), 2.47 (t, *J* = 6.7 Hz, 2H), 1.61 (t, *J* = 8.4 Hz, 1H), 1.50 (m, 2H), 1.41–1.23 (broad overlapping resonance, 16H), 0.88 (t, *J* = 6.6 Hz, 3H).

3-Mercapto-*N*-*n*-dodecylpropionamide C<sub>12</sub>-1AT was synthesized analogously to C<sub>9</sub>-1AT with the substitution of *n*-dodecylamine for *n*-nonylamine and with purification by preparative radial thin-layer chromatography (1 mm rotor, gradient of 25% to 50% ethyl acetate in *n*-hexane). Yield: 70%. Mp: 63.0–64.4 °C. <sup>1</sup>H NMR (300 MHz, CDCl<sub>3</sub>): δ 5.83 (broad, 1H), 3.27 (m, 2H), 2.83 (m, 2H), 2.48 (t, *J* = 6.8 Hz, 2H), 1.61 (t, *J* = 8.3 Hz, 1H), 1.50 (m, 2H), 1.40–1.24 (broad overlapping resonance, 18H), 0.89 (t, *J* = 6.5 Hz, 3H).

3-Mercapto-*N*-*n*-tridecylpropionamide C<sub>13</sub>-1AT was synthesized analogously to C<sub>9</sub>-1AT with the substitution of *n*-tridecylamine for *n*-nonylamine and with purification by preparative radial thin-layer chromatography (1 mm rotor, gradient of 10% to 30% ethyl acetate in *n*-hexane). Yield: 44%. Mp: 67.5–68.7 °C. <sup>1</sup>H NMR (300 MHz, CDCl<sub>3</sub>): δ 5.70 (broad, 1H), 3.27 (m, 2H), 2.83 (m, 2H), 2.47 (t, *J* = 6.8 Hz, 2H), 1.61 (t, *J* = 8.4 Hz, 1H), 1.51 (m, 2H), 1.38–1.23 (broad overlapping resonance, 20H), 0.89 (t, *J* = 6.6 Hz, 3H).

3-Mercapto-*N*-*n*-tetradecylpropionamide C<sub>14</sub>-1AT was synthesized analogously to C<sub>9</sub>-1AT with the substitution of *n*-tetradecylamine for *n*-nonylamine. Yield: 78%. Mp: 68.1–69.2 °C. <sup>1</sup>H NMR (300 MHz, CDCl<sub>3</sub>): δ 5.75 (broad, 1H), 3.26 (m, 2H), 2.82 (m, 2H), 2.47 (t, *J* = 6.7 Hz, 2H), 1.62 (t, *J* = 8.3 Hz, 1H), 1.51 (m, 2H), 1.36–1.22 (broad overlapping resonance, 22H), 0.88 (t, *J* = 6.5 Hz, 3H).

3-Mercapto-*N*-*n*-pentadecylpropionamide C<sub>15</sub>-1AT was synthesized analogously to C<sub>9</sub>-1AT with the substitution of *n*-pentadecylamine for *n*-nonylamine and with purification as for C<sub>12</sub>-1AT. Yield: 67%. Mp: 69.2–69.7 °C. <sup>1</sup>H NMR (300 MHz, CDCl<sub>3</sub>): δ 5.54 (broad, 1H), 3.27 (m, 2H), 2.83 (m, 2H), 2.48 (t, *J* = 6.8 Hz, 2H), 1.62 (t, *J* = 8.4 Hz, 1H), 1.51 (m, 2H), 1.35–1.23 (broad overlapping resonance, 24H), 0.88 (t, *J* = 6.6 Hz, 3H).

3-Mercapto-*N*-*n*-hexadecylpropionamide C<sub>16</sub>-1AT was synthesized analogously to C<sub>9</sub>-1AT with the substitution of *n*-hexadecylamine for *n*-nonylamine and with purification as for C<sub>12</sub>-1AT. Yield: 39%. Mp: 74.5–75.7 °C. <sup>1</sup>H NMR (300 MHz, CDCl<sub>3</sub>): δ 5.68 (broad, 1H), 3.27 (m, 2H), 2.83 (m, 2H), 2.48 (t, *J* = 6.7 Hz, 2H), 1.62 (t, *J* = 8.4 Hz, 1H), 1.51 (m, 2H), 1.35–1.22 (broad overlapping resonance, 26H), 0.89 (t, *J* = 6.5 Hz, 3H).

3-Mercapto-*N*-*n*-octadecylpropionamide C<sub>18</sub>-1AT was synthesized analogously to C<sub>9</sub>-1AT with the substitution of *n*-octadecylamine for *n*-nonylamine and with purification as for C<sub>12</sub>-1AT. Yield: 45%. Mp: 85.7–87.3 °C. <sup>1</sup>H NMR (300 MHz, CDCl<sub>3</sub>): δ 5.81 (broad, 1H), 3.28 (m, 2H), 2.83 (m, 2H), 2.48 (t, *J* = 6.8 Hz, 2H), 1.62 (t, *J* = 8.3 Hz, 1H), 1.51 (m, 2H), 1.35–1.20 (broad overlapping resonance, 30H), 0.89 (t, *J* = 6.6 Hz, 3H).

**Formation of Substrates and SAMs.** Au substrates (1500 Å) with 75 Å Cr adhesion layers were formed on glass slides by evaporation in an Edwards 306A evaporation chamber (base pressure =  $6 \times 10^{-7}$  mbar). The substrates were stored under absolute ethanol until use. Glassware for adsorption and glass slides were cleaned with fresh piranha solution (1:5 30% H<sub>2</sub>O<sub>2</sub> in concentrated H<sub>2</sub>SO<sub>4</sub>; *caution: reacts violently with organic material*). Immediately before soaking in a 1 mM ethanolic solution of the desired thiol, substrates were cleaned for 5 min using a high-intensity Hg lamp (UV Clean, Boekel Industries) in air and rinsed with copious Nanopure (Barnstead) water and absolute ethanol. At least four independent measurements on separate samples were obtained for all data sets.

**X-ray Photoelectron Spectroscopy.** XPS was performed on a Kratos HSi spectrometer as previously described,<sup>9a</sup> with binding energies referenced to Au (4f<sub>7/2</sub>) at 84.0 eV. Thickness was calculated by area integration of the Au (4f<sub>7/2</sub>) peak before and after Ar<sup>+</sup> sputtering for

30 s at takeoff angles of 45° and 30°. Complete film removal was ensured by multiplexing at 300–280 eV (the C(1s) region) after sputtering. The attenuation length  $\lambda$  is 42 Å based on our previous work.<sup>9a</sup>

**Contact Angle Goniometry.** Contact angles were measured using a captive drop technique<sup>14a</sup> on a goniometer constructed in our laboratory.<sup>9a</sup> Advancing and receding contact angles are defined as the maximum and minimum angles formed between the film–droplet interface and the tangent to the probe droplet at its intersection with the substrate.<sup>15</sup>

**Molecular Modeling.** Molecular modeling was performed using Spartan 5.0 (Wavefunction, Inc.) as previously reported.<sup>9a</sup>

**FTIR-ERS.** External reflective IR spectroscopy was performed using a Nicolet Magna 550 IR with a Spectra-Tech 80 fixed reflectance accessory and a Cambridge Physical Sciences IR wire grid polarizer. Spectra were collected as 1024 signal-averaged interferograms as previously reported.<sup>7a</sup> To minimize baseline periodicity and gas-phase water peaks, the amide spectra shown are the Fourier transforms of the interferogram averages of four to six independent samples. Residual gas-phase water was subtracted from these spectra, and minimal automatic baseline correction was applied using the Nicolet software. All spectra shown are unsmoothed.

**Electrochemical Characterization.** A connect between the Au working electrode (ca. 1 cm<sup>2</sup>) and a Teflon shrink-wrapped 22 g solid Cu wire was made with Ag paint (Ted Pella). The exposed Ag, Cu, and Cr surfaces were passivated with epoxy (Dexter). Double-layer capacitance (*C<sub>dl</sub>*) and electrochemical blocking effect (EBE) were measured on a BAS 100 electrochemical workstation using a Pt counter electrode and an SSCE reference electrode.<sup>7a</sup> The electrolyte was 1.0 M KCl (aq). For EBE, the analyte was 1.0 mM K<sub>3</sub>Fe(CN)<sub>6</sub>. The films were electrochemically annealed by the method of Finklea.<sup>17</sup>

## Results

Interpretation of the analytical data leads to a consistent structural description of the monolayer series C<sub>*n*</sub>-1AT/Au (*n* = 9, 11–16, 18). Each of the members of the series has an extensively hydrogen bonded underlayer of amide groups. Adjacent to the amide layer is either an ordered or a disordered hydrocarbon overlayer, depending on the length of the alkyl tails. We will show that the length threshold for alkyl tail ordering is *n* = 15.

**X-ray Photoelectron Spectroscopy (XPS) Shows That Chemisorbed, Anisotropic Monolayers Are Formed.** XPS provides information about the identity, chemical environment, and depth of the constituent elements of these films.<sup>20</sup> The S(2p) peak positions are consistent with covalent attachment to gold,<sup>14a,21</sup> and the remaining SAM peaks occur at energies expected for amide and alkyl material.<sup>7a,22</sup> Due to the attenuation of photoelectrons by overlying material, the relative intensity of C(1s) is enhanced at the expense of the signals from the other atoms.<sup>23</sup> This effect is exaggerated in the longer chain SAMs because the hydrocarbon overlayer is thicker.<sup>8b,12,24</sup> The film thicknesses calculated from XPS intensities agree with those predicted by molecular modeling (Figure 2).<sup>9a</sup>

(20) For comprehensive reviews, see: (a) Briggs, D.; Riviere, J. C.; Hofmann, S.; Seah, M. P. In *Practical Surface Analysis by Auger X-ray Photoelectron Spectroscopy*; Briggs, D., Seah, M. P., Eds.; Wiley & Sons: Chichester, U.K., 1983; pp 87–216. (b) Hochella, M. F., Jr. *Rev. Mineral.* **1988**, *18*, 573–637.

(21) (a) Dubois, L. H.; Zegarski, B. R.; Nuzzo, R. G. *J. Am. Chem. Soc.* **1990**, *112*, 570–579. (b) Nuzzo, R. G.; Dubois, L. H.; Allara, D. L. *J. Am. Chem. Soc.* **1990**, *112*, 558–569.

(22) (a) Bomben, K. D.; Dev, S. D. *Anal. Chem.* **1988**, *60*, 1393–1397. (b) Clark, D. T.; Peeling, J.; Colling, L. *Biochim. Biophys. Acta* **1976**, *453*, 533–545.

(23) Cadman, P.; Evans, S.; Scott, J. D.; Thomas, J. M. *J. Chem. Soc., Faraday Trans. 2* **1975**, *71*, 1777–1784.

(24) Troughton, E. B.; Bain, C. D.; Whitesides, G. M.; Nuzzo, R. G.; Allara, D. L.; Porter, M. D. *Langmuir* **1988**, *4*, 365–385.

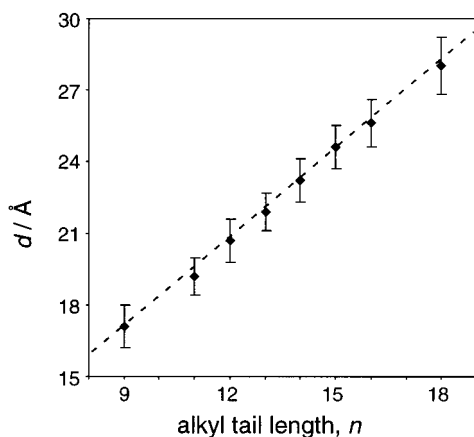


**Figure 2.** Thickness by XPS of SAMs of alkanethiols containing a single internal amide on gold (the series  $C_n$ -IAT/Au). Error bars denote first standard deviation. Dashed line: calculated thicknesses for the amide-containing alkanethiol SAMs of different chain lengths.

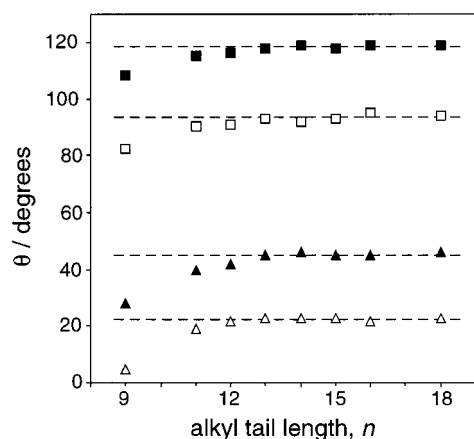


**Figure 3.** Contact angles  $\theta$  for SAMs of the series  $C_n$ -IAT/Au: squares, water; triangles, hexadecane; filled symbols, advancing; open symbols, receding. The dashed lines show the average contact angles for  $n = 13$ – $18$  and are included as guides to the eye. All measurements are  $\pm 2^\circ$ .

**Contact Angle Goniometry Suggests That Order Varies with Alkyl Chain Length.** The hydrophobicity of a surface reflects the degree of order in the top few atomic layers.<sup>21a,24</sup> For  $C_n$ -IAT/Au,  $n \geq 13$ , the contact angle  $\theta$  (Figure 3) is as high as that for well-ordered  $n$ -alkanethiol SAMs,<sup>14a,24</sup> suggesting a maximal degree of order in the amide-containing series above a minimum alkyl chain length. A slight decrease in  $\theta$  consistent with greater disorder at shorter chain lengths is noted for  $n = 11$  and  $12$ , especially using hexadecane, which is more sensitive to disorder than water.<sup>6</sup> The contact angle is substantially decreased for  $n = 9$ , consistent with disordered methyl surfaces.<sup>6,24</sup> The absence of increase in hysteresis below the ordering threshold is addressed in the Discussion.

**Reflective IR (FTIR-ERS) Provides Both Orientational and Conformational Information about the Hydrocarbon Overlayers.** In organic assemblies on reflective substrates, specific information about alkyl chain orientation and order is contained in the frequencies, widths, and relative intensities of the methylene stretching bands.<sup>25</sup> For example, close-packed alkyl chains in  $n$ -alkanethiol SAMs on gold have  $\text{CH}_2(\text{as})$  and  $\text{CH}_2(\text{sym})$  at  $2918$  and  $2950 \text{ cm}^{-1}$ , respectively, representing

small but significant (up to  $6$ – $8 \text{ cm}^{-1}$ ) red shifts compared to disordered films.<sup>14,21,24,26,27</sup> Full widths at half-maxima of  $12 \text{ cm}^{-1}$  for  $\text{CH}_2(\text{as})$  and  $8 \text{ cm}^{-1}$  for  $\text{CH}_2(\text{sym})$  correspond to well-ordered, all-trans chains with a low dispersion of conformational states.<sup>8b,14b</sup> In accordance with the IR surface selection rule, peak intensities are proportional to the dipole components perpendicular to the substrate plane.<sup>28</sup> Thus, the relative intensities of the methylene stretch modes have been used to obtain quantitative information about chain orientation for  $n$ -alkanethiols on gold.<sup>14b,21b,26,29</sup> Such an analysis is not applicable for amide-containing alkanethiols because of uncertainty about the conformation of the ethylene linker between the amide and the sulfur<sup>7a</sup> as well as its contribution to the intensities of the methylene peaks.<sup>14b</sup> However, semiquantitative evaluation of spectra using the parameters described above<sup>8b,14,21b,24,26,27</sup> and qualitative comparisons to SAMs with known structures<sup>8b,9b,10,12,24,30</sup> are useful in evaluating film order.

**The Alkyl Region Is Well-Ordered When  $n \geq 15$ , but Shorter SAMs have Disordered Chains.** The reflective IR spectra (Figure 4) for  $C_{15}$ -tailed one-amide precursors show that a well-ordered hydrocarbon overlayer forms and that the SAMs are even more highly ordered for  $n \geq 16$ . For the latter films, the  $\text{CH}_2(\text{as})$  and  $\text{CH}_2(\text{sym})$  frequencies,<sup>14,21b,24,26,27</sup> intensities,<sup>14b,21b,26,29</sup> and bandwidths<sup>8b,14b,21b,26,29</sup> match those of very highly ordered  $n$ -alkanethiol SAMs. As chain length decreases, the first hint of decreased order comes from the decreased intensity of the  $\text{CH}_2$  peaks in  $C_{15}$ -IAT/Au. However, the low peak frequencies and widths, as well as comparison to  $C_{15}\text{S/Au}$ <sup>26</sup> (which is highly ordered), indicate that  $C_{15}$ -IAT/Au is well-ordered.

In contrast, the alkyl overlayers in  $C_n$ -IAT/Au with  $n = 11$ – $14$  are disordered. For these chain lengths, peaks due to methylene stretching modes are weak, broadened, and blue shifted. Although the weak intensities (Figure 5) are consistent either with general disorder<sup>28</sup> or a gradual loss of linearity between peak intensity and C–H(str) dipole orientation,<sup>14b</sup> the blue shifts<sup>14,21b,24,26,27</sup> and broadening<sup>8b,14b</sup> are consistent only with disorder.

The breakdown of quantitative reflective IR for very short alkyl chains has been previously observed in  $n$ -alkanethiol SAMs and has been attributed to an optoelectronic interaction between methylene dipoles and metal electrons at a polarizable interface.<sup>14b</sup> It is unlikely that the absence of methylene peaks in the  $C_9$ -IAT/Au spectra is evidence of close-packed chains constrained vertically by decreased amide spacing because peaks due to the amide dipoles are identical throughout the series. The quantitative use of reflective IR for C–H(as) and C–H(sym) intensities is not universally reliable;<sup>8a,14b</sup> indeed the data show that the method is unreliable for  $C_9$ -tailed one-amide SAMs. Thus, a complementary characterization method is required to test the structure of the hydrocarbon matrix for  $n = 9$ – $14$ . Such a method is provided by electrochemical techniques (vide infra).

**The IR Data Also Shows That the Amide Underlayers in All of the SAMs Are Well-Ordered and Extensively Hydrogen Bonded.** In contrast to the two types of alkyl regions, the spectra indicate that the amide groups of the entire series are

(26) Laibinis, P. E.; Whitesides, G. M.; Allara, D. L.; Tao, Y.-T.; Parikh, A. N.; Nuzzo, R. G. *J. Am. Chem. Soc.* **1991**, *113*, 7152–7167.

(27) Snyder, R. G.; Strauss, H. L.; Elliger, C. A. *J. Phys. Chem.* **1982**, *86*, 5145–5150.

(28) (a) Greenleer, R. G. *J. Chem. Phys.* **1966**, *44*, 310–316. (b) Francis, S. A.; Ellison, A. H. *J. Opt. Soc. Am.* **1959**, *49*, 131–138. (28) (c) Pearce, H. A.; Sheppard, N. *Surf. Sci.* **1976**, *59*, 205–217.

(29) (a) Allara, D. L.; Nuzzo, R. G. *Langmuir* **1985**, *1*, 52–65. (b) Parikh, A. N.; Allara, D. L. *J. Chem. Phys.* **1992**, *96*, 927–945.

(25) For comprehensive reviews, see: (a) Crooks, R. M.; Xu, C.; Sun, L.; Hill, S. L.; Ricco, A. J. *Spectroscopy* **1993**, *8*, 29–39. (b) Porter, M. D. *Anal. Chem.* **1988**, *60*, 1143A–1155A.

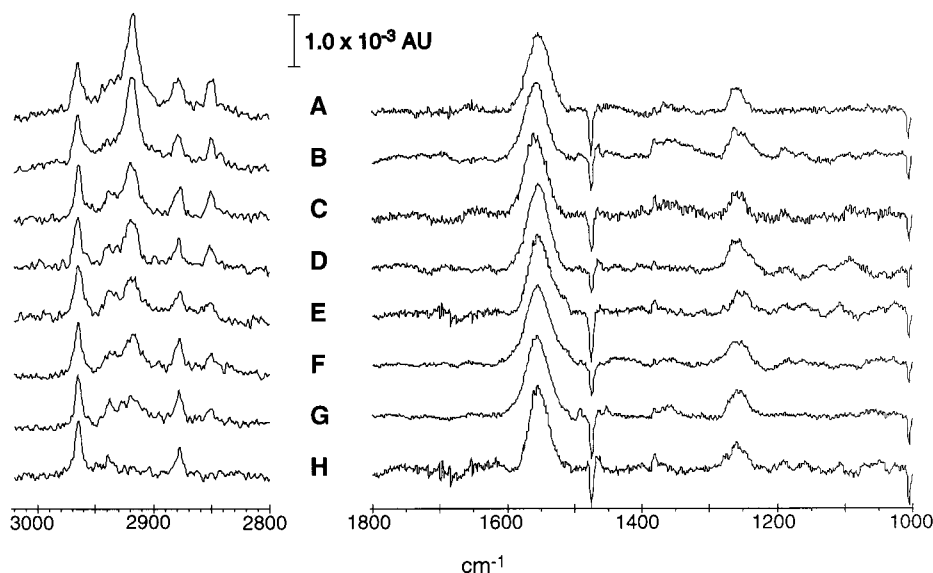


**Figure 4.** FTIR-ERS spectra of SAMs of alkanethiols containing a single internal amide on gold: left, high-frequency C–H(str) region; right, mid-frequency region (amides I, II, and III). (A) C<sub>18</sub>-1AT/Au. (B) C<sub>16</sub>-1AT/Au. (C) C<sub>15</sub>-1AT/Au. (D) C<sub>14</sub>-1AT/Au. (E) C<sub>13</sub>-1AT/Au. (F) C<sub>12</sub>-1AT/Au. (G) C<sub>11</sub>-1AT/Au. (H) C<sub>9</sub>-1AT/Au.

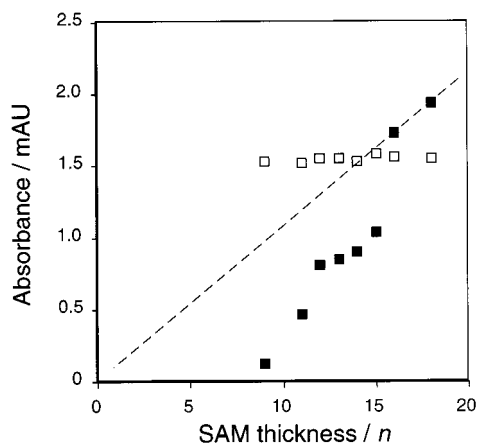


**Figure 5.** Intensities of FTIR-ERS peaks that are important indicators of adsorbate orientation and order. Peak intensities are shown as a function of alkyl chain length  $n$  for the series C <sub>$n$</sub> -1AT/Au: filled symbols, CH<sub>2</sub>(as); open symbols, amide II. The dashed line through the data points at  $n = 16$  and  $18$  is included as an aid to the eye (see text).

oriented with C=O and N–H bonds nearly parallel to the substrate plane. Two diagnostic signals, amide A (N–H(str),  $\sim 3300$  cm<sup>-1</sup>) and amide I (C=O(str),  $\sim 1640$  cm<sup>-1</sup>),<sup>31</sup> are absent or very weak and broad in the SAM spectra. In accordance with the surface selection rule, these weak intensities are consistent with C=O and N–H bonds nearly parallel to the substrate plane.<sup>7a,9,10,12,32</sup>

The dominant feature in the amide region is the amide II peak at  $\sim 1560$  cm<sup>-1</sup>, consisting mainly of N–H(ipb).<sup>31</sup> The high intensity of this peak (along with the weak or absent amides A and D) indicates that this dipole oscillates nearly perpendicular to the substrate plane.<sup>7a,9,12,10,32</sup> Importantly, the amide II bandwidths (Figure 4) and intensities (Figure 5) are constant among the spectra, indicating the amide underlayer (unlike the

alkyl overlayer) is essentially invariant for the series. The high frequency of the amide II peak is consistent with a high degree of hydrogen bonding, as the oscillator frequency follows the degree of constraint placed by an associated carbonyl on the N–H(bend) vibration.<sup>7a,32a,33</sup>

Amide III occurs as a broad peak at  $\sim 1250$  cm<sup>-1</sup>, supporting a trans conformation as expected for a secondary amide group.<sup>9b,31a,b</sup> The primary components of amide III are C–N(str) and N–H(ipb),<sup>31a,b</sup> both of which contain large vectors parallel to the long molecular axis. The extinction coefficient of amide III is low compared to that of amide II,<sup>31a,b</sup> accounting for the decreased intensity of amide III compared to amide II. The amide IR data thus uniformly support the adsorbate orientations depicted in Figure 1A,C and are consistent with the XPS and contact angle data described above.

**Microscopic Defects Such as Pinholes and Disordered Chains Do Not Significantly Contribute to Electron Transfer across Amide-Containing SAMs.** Using the gold substrate and the associated SAM as a working electrode in an electrochemical cell provides further structural information about the SAM. Due to the molecular scale of electron transfer (ET) and charge storage (capacitive) processes, voltammetric techniques reflect molecular order and disorder better than any of the previously discussed methods, enabling discrimination between various types of SAM defects.<sup>1g</sup>

In the electrochemical blocking experiment, the ability of a dielectric layer to block ET between a dissolved redox probe and the electrode is determined from a cyclic voltammogram (CV). A systematic qualitative comparison of CVs often enables differentiation among the three possible mechanisms for ET at a SAM-covered electrode, which are in turn related to various types of SAM defects that may be present.<sup>1g</sup> (1) *Radial diffusion-limited ET* yields a sigmoidal increase in current near  $E^{\circ}$  to a plateau at significant overpotentials and is characteristic of

(30) Tsao, M.-W.; Hoffman, C. L.; Rabolt, J. F.; Johnson, H. E.; Castner, D. G.; Erdelen, C.; Ringsdorf, H. *Langmuir* **1997**, *13*, 4317–4322.

(31) (a) Krimm, S.; Bandekar, J. *J. Adv. Protein Chem.* **1986**, *38*, 181–364. (b) Cheam, T. C.; Krimm, S. *J. Chem. Phys.* **1985**, *82*, 1631–1641. (c) Dwivedi, A. M.; Krimm, S. *Macromolecules* **1982**, *15*, 177–185. (d) Dwivedi, A. M.; Krimm, S. *Biopolymers* **1982**, *21*, 2377–2397.

(32) (a) Sabapathy, R. C.; Bhattacharyya, S.; Leavy, M. C.; Cleland, W. E., Jr.; Hussey, C. L. *Langmuir* **1998**, *14*, 124–136. (b) Strong, A. E.; Moore, B. D. *Chem. Commun.* **1998**, 473–474. (c) Yamada, N.; Koyama, E.; Imai, T.; Matsubara, K.; Ishida, S. *Chem. Commun.* **1996**, 2297–2298. (d) Cha, X.; Ariga, K.; Kunitake, T. *Bull. Chem. Soc. Jpn.* **1996**, *69*, 163–168.

(33) Bamford, C. H.; Elliott, A.; Hanby, W. C. *Synthetic Polypeptides: Preparation, Structure and Properties*; Academic: New York, 1956; pp 193–194.

microelectrode arrays (i.e., widely spaced pinholes<sup>34</sup> less than  $\sim 1 \mu\text{m}$  in diameter).<sup>36</sup> (2) *Linear diffusion-limited ET* results in current decay at potentials beyond the peak potential. Such a CV is characteristic of a film with large or closely spaced pinholes<sup>34</sup> or that is highly permeable to redox probe<sup>14b,37</sup> (corresponding to extreme disorder, hydrophilicity, or poor coverage<sup>34</sup>). (3) *Kinetically limited ET* yields a quasiexponential current rise with increasing overpotential,<sup>38</sup> consistent with a through-chain mechanism of ET occurring at a nearly defect-free SAM.<sup>14b,37b,39</sup>

In a complementary and more quantitative treatment of electrochemical blocking CVs, the electrochemical blocking effect (EBE) is calculated as

$$\text{EBE} = 1 - (i_{1/2(\text{film})}/i_{1/2(\text{bare})}) \quad (1)$$

where  $i_{1/2}$  denotes the Faradaic current (total current less charging current) for a SAM-covered and bare electrode (each measured at the half-wave potential recorded for the bare electrode).<sup>40a</sup> A value of EBE near unity indicates that kinetically limited ET predominates, as a significant component of either radial or linear diffusion-limited ET will sharply increase the measured  $i_{1/2(\text{film})}$ .<sup>40</sup> A more stringent test of the absence of diffusion limited ET is provided by measuring the Faradaic currents at different potential scan rates. For nearly defect-free SAMs in which kinetically limited ET predominates, the Faradaic current should be independent of scan rate.<sup>38</sup>

All of the SAMs in the series  $C_n$ -1AT/Au yield kinetically limited voltammograms<sup>14b,37b,39</sup> (Figure 6), indicating that neither film permeation by analyte<sup>14b,37</sup> nor diffusion of analyte to pinholes<sup>36</sup> plays a significant role in ET. Thus, ET is limited primarily to through-chain electronic coupling,<sup>14b,37b,39</sup> the density of pinholes is insignificant,<sup>14b,36</sup> and the substrate is well-covered with adsorbate.<sup>14b,37</sup> This interpretation is supported by

(34) For the purpose of this analysis, we adopt three general *functional* classes of SAM defects. (i) *Pinholes* are bare spots large enough for analyte to participate in unmediated ET at the electrode surface.<sup>35</sup> These include large areas of bare electrode, missing rows of adsorbate, and single missing adsorbate molecules. At pinholes, analyte can approach the electrode closely enough to undergo direct ET, so the EBE is sharply reduced if the total pinhole area is significant.<sup>14b,35</sup> (ii) *Disordered domains* are areas of high coverage into which electrolyte (and possibly analyte, depending on coverage) can permeate due to adsorbate disorder.<sup>14b</sup> ET from analyte coupling to the electrode nearly across the full thickness of the SAM is far slower than at pinholes (because the ET rate decreases exponentially with distance), so if chain density is high enough that analyte neither approximates the metal surface nor diffuses freely through the film,<sup>14b</sup> then disorder of the alkyl overlayer reduces EBE the least of these defect types. (iii) Intermediate cases include *point defects* and *grain boundaries*,<sup>18</sup> where adsorbate molecules in neighboring domains tilt away from each other. If such defects extend to the level of the sulfur atoms, the effect on electrochemical blocking behavior will resemble that of pinholes.<sup>18</sup> However, if such defects extend only to the base of the hydrocarbon overlayer, such that the hydrogen bonding amide layer is not disrupted and electronic coupling must occur through a significant part of the chain, the effect will tend toward that of disordered domains.<sup>18</sup>

(35) Stranick, S. J.; Parikh, A. N.; Allara, D. L.; Weiss, P. S. *J. Phys. Chem.* **1994**, *98*, 11136–11142.

(36) (a) Dayton, M. A.; Brown, J. C.; Stutts, K. J.; Wightman, R. M. *Anal. Chem.* **1980**, *52*, 946–950. (b) Gao, Z.; Siow, K. S. *Electrochim. Acta* **1997**, *42*, 315–321.

(37) (a) Ikeda, T.; Schmehl, R.; Denisevich, P.; Willman, K.; Murray, R. W. *J. Am. Chem. Soc.* **1982**, *104*, 2683–2691. (b) Chidsey, C. E. D.; Loiacono, D. N. *Langmuir* **1990**, *6*, 682–691.

(38) Miller, C.; Grätzel, M. *J. Phys. Chem.* **1991**, *95*, 5225–5233.

(39) (a) Cheng, J.; Sági-Szabó, G.; Tossell, J. A.; Miller, C. J. *J. Am. Chem. Soc.* **1996**, *118*, 680–684. (b) Slowinski, K.; Chamberlain, R. V.; Miller, C. J.; Majda, M. *J. Am. Chem. Soc.* **1997**, *119*, 11910–11919.

(40) (a) Chen, C.-h.; Hutchison, J. E.; Postlethwaite, T. A.; Richardson, J. N.; Murray, R. W. *Langmuir* **1994**, *10*, 3332–3337. (b) Aslanidis, D.; Fransaer, J.; Celis, J.-P. *J. Electrochem. Soc.* **1997**, *144*, 2352–2357. (c) Skoog, M.; Kronkvist, K.; Johansson, G. *Anal. Chim. Acta* **1992**, *269*, 59–64. (d) Hrbek, J. *J. Phys. Chem.* **1986**, *90*, 6217–6222.

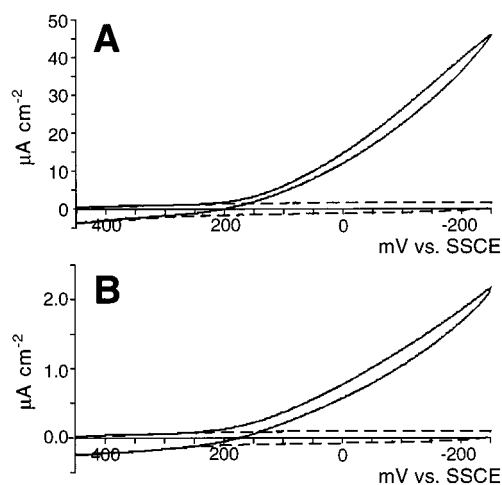


**Figure 6.** Representative cyclic voltammograms from the electrochemical blocking and double layer capacitance experiments on SAMs of alkanethiols containing a single internal amide on gold (scan rate = 100 mV/s; SSCE reference electrode): solid lines, 1.0 mM  $\text{K}_3\text{Fe}(\text{CN})_6$  in 1.0 M KCl; dashed lines, 1.0 M KCl. (A)  $C_9$ -1AT/Au. (B)  $C_{18}$ -1AT/Au.

**Table 1.** Double-Layer Capacitance and Electrochemical Blocking Effect for SAMs of Alkanethiols Containing a Single Internal Amide on Gold<sup>a</sup>

	$C_{dl}^b$ ( $\mu\text{F}/\text{cm}^2$ )	EBE <sup>c</sup>
$C_9$ -1AT/Au	$13.7 \pm 0.8$	$0.9985 \pm 0.0003$
$C_{11}$ -1AT/Au	$8.0 \pm 0.5$	$0.9988 \pm 0.0004$
$C_{12}$ -1AT/Au	$5.9 \pm 0.3$	$0.9989 \pm 0.0003$
$C_{13}$ -1AT/Au	$4.5 \pm 0.2$	$0.9993 \pm 0.0002$
$C_{14}$ -1AT/Au	$2.8 \pm 0.2$	$0.9994 \pm 0.0003$
$C_{15}$ -1AT/Au	$1.03 \pm 0.04$	$0.9996 \pm 0.0002$
$C_{16}$ -1AT/Au	$1.00 \pm 0.05$	$0.9996 \pm 0.0002$
$C_{18}$ -1AT/Au	$0.91 \pm 0.03$	$0.9998 \pm 0.0001$
$C_{18}\text{S}/\text{Au}$	$0.97 \pm 0.06$	$0.9995 \pm 0.0003$

<sup>a</sup> SSCE reference electrode. Our measurements for octadecanethiol SAMs on gold ( $C_{18}\text{S}/\text{Au}$ ) are included for comparison to literature values (see ref 14b). <sup>b</sup>  $C_{dl}$  = double-layer capacitance, as defined in eq 3; 1.0 M KCl, scan rate 100 mV/s. <sup>c</sup> EBE = electrochemical blocking effect at  $E^\circ$ , as defined in eq 1 (0 = bare electrode; unity = fully blocking electrode); 1.0 mM  $\text{K}_3\text{Fe}(\text{CN})_6$  in 1.0 M KCl, scan rate 50–500 mV/s.

the measured EBE values, which approach unity for all the SAMs (Table 1) and indicate that direct ET between analyte and metal is minimal.<sup>40</sup> EBE is independent of scan rate (Table 1), further supporting kinetically limited ET, high adsorbate coverage, and a low pinhole density.<sup>38</sup>

The EBE data also indicate that ordered and disordered alkyl regions are present in the films of different lengths. The slight but significant decrease in EBE with chain length (Table 1) is consistent with decreased order for the shorter chains.<sup>14b,37</sup> With low pinhole density and high coverage, the amount of ET occurring by a through-chain mechanism can increase in disordered films because the redox probe can access portions of the chains inside the terminal methyl groups.<sup>14b,37</sup> The observed EBE data are thus consistent with the alkyl IR data which indicate disordered hydrocarbon chains for  $n \leq 14$ . A more sensitive indication of the degree of alkyl order in films known to have low pinhole densities is obtained from double-layer capacitance measurements, as described next.

**Capacitance Measurements Indicate That the Alkyl Chains Are Close-Packed in  $C_n$ -1AT/Au for  $n \geq 15$ .** Another useful parameter describing SAM characteristics is the double-layer capacitance ( $C_{dl}$ ) because a well-ordered SAM in the absence of redox probe approximates the behavior of an ideal capacitor.<sup>18</sup>

The magnitude of  $C_{dl}$  reflects the extent of the electrical double layer formed at the electrode surface.<sup>41a</sup> If the SAM contains significant defects such as pinholes<sup>34</sup> or disordered chains,<sup>34</sup> electrolyte should penetrate into the film, resulting in a more extensive double layer and a high  $C_{dl}$ .<sup>14b,38,41</sup> However, if the SAM is impermeable to electrolyte,  $C_{dl}$  is low.  $C_{dl}$  is more sensitive than EBE to the presence of disordered chains due to selectivity of disordered domains for small ions of high charge density (e.g.,  $K^+$  and  $Cl^-$  as used in  $C_{dl}$  measurements) over large ions (e.g.,  $Fe(CN)_6^{3-}$ , the redox probe used in EBE experiments).<sup>14b</sup> The sensitivity of  $C_{dl}$  is of course enhanced if the pinhole area (from EBE) is low.

As predicted by the Helmholtz parallel plate capacitor model,<sup>42</sup>  $C_{dl}$  in well-ordered SAMs varies inversely with film thickness  $d$  as

$$C_{dl}^{-1} = d(\epsilon\epsilon_0)^{-1} \quad (2)$$

in which  $C_{dl}$  is determined from the measured charging current  $i_c$  according to

$$C_{dl} = i_c(\nu A)^{-1} \quad (3)$$

where  $\nu$  is scan rate and  $A$  is electrode surface area. For example, in ordered  $n$ -alkanethiol SAMs ( $C_nS/Au$ ,  $n \geq 12$ ), eq 2 yields a linear plot with slope corresponding to the apparent dielectric constant  $\epsilon$  of the SAM.<sup>14b,39b</sup> Disordered  $n$ -alkanethiol SAMs ( $n < 12$ ) exhibit capacitances larger than predicted by the model, consistent with film permeation by charge carriers.<sup>14b</sup>

In the amide-based series, a gradual decrease in  $\epsilon$  is expected with a decreasing proportion of amide to alkyl material. Thus, amide-containing SAMs with short alkyl chains may deviate from the ideal line for two reasons: (1) permeation of a disordered alkyl overlayer by electrolyte and/or solvent (adding a diffuse layer component to the monolayer capacitance) and (2) an increase in  $\epsilon$  with the increase in relative amide component. At long chain lengths, however, the proportion of amide material in the films is nearly constant among different chain lengths. This allows another measure of order in the SAMs, as the actual monolayer capacitances can be tested against those predicted by the model for ordered films.

For the amide-containing SAMs with  $n \geq 15$ ,  $C_{dl}$  is comparable to that of  $C_{18S/Au}$  ( $1.0 \mu F cm^{-2}$ ) (Table 1). The slope of the regression line for  $n \geq 15$  yields  $\epsilon = 3.3 \pm 0.8$  (Figure 7), which compares favorably to Nylon-6,6 ( $\epsilon = 3.6$ )<sup>43a</sup> and polyethylene ( $\epsilon = 2.3$ ),<sup>43b</sup> as well as to the ordered  $C_nS/Au$  series (for which the slope yields  $\epsilon = 2.3$  using a chain tilt of  $28^\circ$ ).<sup>14b</sup> The conformity to the model supports impermeability of the long-chain SAMs to ions and solvent as expected for

(41) (a) Bard, A. J.; Faulkner, L. R. *Electrochemical Methods: Fundamentals and Applications*; Wiley & Sons: New York: 1980; pp 488–511. (b) Becka, A. M.; Miller, C. J. *J. Phys. Chem.* **1993**, *97*, 6233–6239.

(42) The empirically measured capacitance is actually the total interfacial capacitance  $C_T$  which is treated by Guoy–Chapman–Stern theory as two series capacitances: (i) the double-layer capacitance  $C_{dl}$  and (ii) the capacitance of the diffuse layer of electrolyte  $C_d$ . In the case of a SAM-covered electrode,  $C_{dl}$  is equivalent to the monolayer capacitance  $C_m$ , the parameter of interest for examining charge storage at the SAM–electrolyte interface.  $C_T$  provides an excellent approximation of  $C_m$  because  $C_d > 200 \mu F cm^{-2}$  in 1.0 M aqueous electrolyte near the potential of zero charge.<sup>14b,41b</sup> and

$$C_T^{-1} = C_m^{-1} + C_d^{-1}$$

It follows that the contribution of  $C_d$  to  $C_T$  is vanishingly small in this system, with  $i_c$  measured at +150 mV vs SSCE.

(43) (a) Dasgupta, S.; Hammond, W. B.; Goddard, W. A., III. *J. Am. Chem. Soc.* **1996**, *118*, 12291–12301. (b) Lanza, V. L.; Herrman, D. B. *J. Polym. Sci.* **1958**, *28*, 622–625.

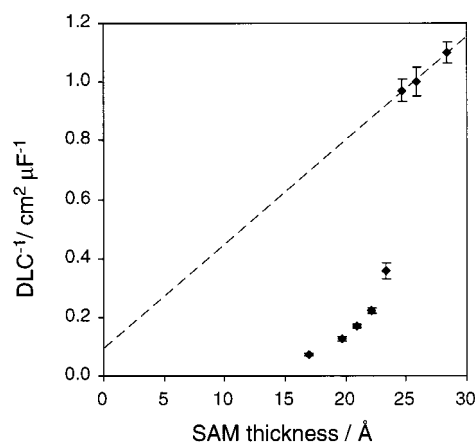


**Figure 7.** Plot of reciprocal capacitance as a function of SAM thickness (scan rate = 100 mV/s; 1.0 M KCl electrolyte). Error bars denote first standard deviation. The dashed line is the regression line for  $n = 15$ , 16, and 18.

close-packed, well-ordered films. For the shorter monolayers ( $n \leq 14$ ),  $C_{dl}$  falls off precipitously as chain length is decreased, indicating a sharp transition in either chain packing or  $\epsilon$  of the adsorbate. The latter is unreasonable as noted above because the change in material composition with chain length is gradual. The deviation from the model indicates that a more extensive electrical double layer forms than expected for  $n \leq 14$ , consistent with monolayer permeability to ions or solvent. Therefore, the electrochemical capacitance measurements and the FTIR-ERS data both support an alkyl overlayer ordering threshold at  $n = 15$  in  $C_n$ -1AT/Au.

## Discussion

The adsorption of  $C_n$ -1AT ( $n = 9, 11–16, 18$ ) onto gold substrates yields chemisorbed monolayers with the following structural features: (1) well-ordered amide layers with extensive hydrogen bonding for all alkyl chain lengths, (2) disordered alkyl domains in SAMs with short chains ( $n \leq 14$ ), and (3) close-packed, tilted alkyl domains in SAMs with long chains ( $n \geq 15$ ). This structural interpretation is consistent with all results from XPS, contact angle goniometry, FTIR-ERS, and capacitance and electrochemical blocking studies.

**The Alkyl Chain Length Ordering Threshold in the One-Amide SAMs Is Approximately  $n = 15$ .** Based on the data, alkyl chain length clearly determines whether the hydrocarbon region is ordered or disordered. The results from the various techniques must be evaluated by an integrated approach, and appropriate comparisons to structurally related systems are required.<sup>44</sup>

As characterized by reflective IR the chains are well-ordered at  $n = 15$  and very highly ordered at  $n \geq 16$ , but according to  $C_{dl}$ , the chains are ordered at  $n \geq 15$ . This apparent discrepancy

(44) The synergy of the multiple characterization methods used in this study leads to a stronger case for the structures proposed than if only one or two of the methods were considered. Errors in this regard are not uncommon and can lead to unfounded conclusions. We note in particular a recent study<sup>11</sup> in which similar amide-containing sublayers were covalently bonded to propyl through heptyl tails. The use of limited characterization techniques and the evaluation of the results without consideration of known principles of  $n$ -alkanethiol and amide-based alkanethiol SAM structure led to two apparently erroneous conclusions: (i) that amide underlayers in the heptyl- and propyl-tailed films differ from each other and (ii) that heptyl chains are ordered whereas propyl ones are not. The first conclusion is not supported by differences in the amide IR peaks shown in that report,<sup>11</sup> and the second is inconsistent with the  $C_{dl}$  and contact angle data presented here as well as with evidence that reflective IR does not reliably indicate orientation for short alkyl chains.<sup>14b</sup>

arises from differences in the two techniques.  $C_{dl}$  measures the effect of the monolayer on the interaction of electrolyte and electrode,<sup>41a,1g</sup> whereas reflective IR directly measures a physical property of the adsorbate.<sup>25</sup> Due to the hydrophobicity of hydrocarbon chains, a difference of one methylene between  $C_{dl}$  and FTIR-ERS is reasonable in view of the polarity of the environments (aqueous electrolyte vs dinitrogen respectively).

The threshold for order in the contact angle plot at  $n = 13$  occurs at shorter chain lengths than indicated by FTIR-ERS and  $C_{dl}$ . Of the characterization techniques used here, contact angle goniometry is the least sensitive to disorder. For example, in *n*-alkanethiol SAMs the onset of contact angle decrease<sup>6,14,21a,24</sup> is two to four methylenes below the ordering threshold established by diffraction methods.<sup>45a-d</sup> This comparison explains the difference in the ordering threshold indicated by contact angle goniometry compared to the other techniques. Also, the hysteresis (difference between advancing and receding contact angles) does not change as expected for measurements in the vicinity of an ordering threshold.<sup>24</sup> For both of these reasons, we view contact angle goniometry as a useful screening technique that is less reliable for detailed studies of order and disorder in monolayer films than FTIR-ERS and measurement of  $C_{dl}$ .

**A Higher Alkyl Chain Length Ordering Threshold Exists in One-Amide Than in *n*-Alkanethiol SAMs.** In ordered  $C_nS/Au$  films, the threshold chain length is known to be  $n = 10-12$ ,<sup>45a-d</sup> several methylenes shorter than in the amide-based SAMs. Thus, *an amide region destructively interferes with close packing of alkyl chains in one-amide SAMs* in comparison to *n*-alkanethiol SAMs. In *n*-alkanethiol SAMs, the structure is templated by the Au (111) lattice.<sup>45</sup> Our results suggest that, in the amide-containing SAMs studied, other interactions dominate over Au-S epitaxy in establishing the assembly structure.

The difference in chain length threshold indicates a sensitivity of hydrocarbon ordering to some difference between the respective "templates." Three general differences between an amide underlayer and a gold-sulfur array may contribute to the change in chain length threshold. (1) A difference between the interamide spacing in an amide underlayer and the sulfur-sulfur spacing in an *n*-alkanethiol SAM<sup>26</sup> likely changes the steric constraints on the alkyl overlayer. The average sulfur-sulfur spacing of 4.97 Å in *n*-alkanethiols<sup>45d</sup> is replaced by the ~5.1 Å amide cross section in the amide-based series,<sup>9b</sup> assuming similarity of the adsorbate unit cell to that of the structurally analogous *N*-methylacetamide.<sup>31b</sup> Any difference in mismatch between head group and alkyl chain cross sections likely changes the stabilization per hydrophobic interaction, as discussed below.<sup>14a,45c,46</sup> (2) As a result of a difference in head group cross section, the orientation and/or torsional angle of the N-C $\alpha$  bond in an amide-based SAM is likely different from that of the S-C $\alpha$  bond in an *n*-alkanethiol SAM.<sup>1c</sup> Any change in the constraints upon the nitrogen-carbon bond at the amide-alkyl interface obviously alters the geometric considerations for maximizing the energetics of the hydrophobic interactions.<sup>14a,45c,46</sup> (3) Additionally, possible electronic effects arising from differences in template polarizability, dipole moment, or dielectric

constant could affect the hydrocarbon ordering process, as suggested by recent work by Ulman et al.<sup>47</sup>

**The Amide Region Dominates in Establishing the Structure of These Monolayers.** All the characterization data are consistent with the presence of amide underlayers that are well-ordered and extensively hydrogen bonded, independent of variations in alkyl packing. This directly indicates *spacing and order of the amide "template" are not affected by changes in hydrocarbon orientation and order*. It also suggests that the hydrophobic interactions exert little influence on the degree of hydrogen bonding in these films. In this way, alkanethiol SAM stability may be enhanced by introducing hydrophilic cross-linking interactions, as has been suggested by other authors.<sup>3c,9b,12</sup> We previously reported results supporting this effect.<sup>9a</sup> Such stability in short-chain SAMs is desired for improved conductometric sensor design.<sup>48</sup>

A likely reason hydrogen bonding dominates over gold-sulfur templating (as in *n*-alkanethiol SAMs) in determining these film structures is that the possible cost in free energy of a gold-sulfur lattice mismatch is offset by replacing hydrophobic interactions (0.6-1.6 kcal/mol<sup>14a,45c</sup>) with N-H-O hydrogen bonds (3-5 kcal/mol<sup>7a,9b,31a</sup>). Two types of gold-sulfur lattice mismatches are possible. (1) All sulfur may be bound to 3-fold gold hollow sites via the  $sp^3$  mode characteristic of *n*-alkanethiol SAMs.<sup>45c-e</sup> Mismatch between the Au(111) lattice and the amide lattice would be accommodated by variations in the conformations of the ethylene linkers<sup>7a</sup> between the sulfur and the amide groups (e.g., at an increase in enthalpy of only ~0.8 kcal/mol for a change from *trans* to *gauche*<sup>49</sup>) and by occasional skips in the 3-fold hollow binding pattern. (2) Multiple sulfur-gold bonding geometries or sites would also allow the sulfur-gold templating to relax in favor of the hydrogen bonding lattice parameters. Different modes are certainly accessible, as both  $sp^3$  and  $sp$  bonding modes have been observed in alkanethiol<sup>45c-e</sup> and aryl thiol<sup>50a</sup> SAMs, respectively. Previous studies have calculated a potential energy difference of 0.4 kcal/mol between these modes,<sup>1c</sup> and a spectrum of binding sites and geometries may exist on the Au-(111) surface.<sup>50b</sup> The actual binding motif at the organic-metal interface may contain elements of each of these binding modes. Elucidation of these details awaits direct structural analysis by XRD, helium diffraction, or STM.

**The Independence of Amide Structure from Hydrocarbon Packing Demonstrates "Rigid-Elastic" Behavior at the Amide-Alkyl Interface.** A recent grazing incidence XRD study of  $C_nS/Au$  assemblies ( $n = 10-30$ ) revealed gradual trends in tilt angle and direction as a function of  $n$ . This was explained by an interplay between variable intermolecular interactions and fixed substrate-monolayer interactions.<sup>45a-b</sup> Such a rigid-elastic interface differs fundamentally from "rigid-rigid" interfaces as found in epitaxially grown metal-metal films, which exhibit sharp transitions between invariant regimes.

Here we find that *the amide-alkyl interface of one-amide SAMs provides an example of a rigid-elastic buried organic*

(45) (a) Camillone, N., III; Chidsey, C. E. D.; Liu, G.; Scoles, G. *J. Chem. Phys.* **1993**, *98*, 3503-3511. (b) Camillone, N., III; Leung, T. Y. B.; Scoles, G. *Surf. Science* **1997**, *373*, 333-349. (c) Fenter, P.; Eberhardt, A.; Liang, K. S.; Eisenberger, P. *J. Chem. Phys.* **1997**, *106*, 1600-1608. (d) Fenter, P.; Eberhardt, A.; Eisenberger, P. *Science* **1994**, *266*, 1216-1218. (e) Strong, L.; Whitesides, G. M. *Langmuir* **1988**, *4*, 546-558. (f) Poirier, G. E.; Tarlov, M. *J. Langmuir* **1994**, *10*, 2853-2856.

(46) Nuzzo, R. G.; Zegarski, B. R.; Dubois, L. H. *J. Am. Chem. Soc.* **1987**, *109*, 733-740.

(47) Kang, J. F.; Liao, S.; Jordan, R.; Ulman, A. *J. Am. Chem. Soc.* **1998**, *120*, 9662-9667.

(48) Murray, R. W. In *Chemical Sensors and Microinstrumentation*; Murray, R. W., Dessy, R. E., Heineman, W. R., Janata, J., Seitz, W. R., Eds.; ACS Symposium Series 403; American Chemical Society: Washington, DC, 1989; pp 2-3.

(49) Carey, F. A.; Sundberg, R. J. *Advanced Organic Chemistry: Part A, Structure and Mechanisms*, 3rd ed.; Plenum: New York, 1990; pp 121-122.

(50) (a) Sabatani, E.; Cohen-Boulakia, J.; Bruening, M.; Rubinstein, I. *Langmuir* **1993**, *9*, 2974-2981. (b) Sellers, H.; Ulman, A.; Shnidman, Y.; Eilers, J. E. *J. Am. Chem. Soc.* **1993**, *115*, 9389-9401.

interface. The amide region is ordered in all cases, and the hydrocarbon overlayer is ordered only for  $n \geq 15$ . Thus, the amide region acts as a structured "template" upon which the preattached hydrocarbon chains interact with each other laterally via van der Waals forces. Analogous to *n*-alkanethiols, these chains will become ordered if they are long enough to generate sufficient hydrophobic interactions. However, a different templating occurs in the amide-containing SAMs compared to *n*-alkanethiol ones, as evidenced by the higher ordering threshold. Above this threshold, each assembly structure presumably finds a unique energetic minimum for each chain length. Below the minimum number of hydrophobic interactions, disorder results, but the rigid amide "template" is essentially unaffected.

**The Relationships among Amide-Containing Alkanethiol SAMs Have Implications for Other Systems in Which Interactions between Hydrophilic and Hydrophobic Domains Are Important.** It should be noted that the rigid-elastic nature of one-amide-containing SAMs is not common to all amide-containing alkanethiol SAMs. In similar SAMs with two amide groups per precursor, the interplay between the amide and alkyl regions drives the ordering of *both* regions above a certain alkyl threshold (corresponding to a transition from Figure 1B to Figure 1A).<sup>13</sup> Thus, the two-amide SAMs provide examples of a previously unobserved elastic-elastic interface. However, SAMs with three amide groups behave similarly to those with one amide, except that the amide region assumes a different rigid conformation.<sup>13</sup> Thus, in this general class of SAMs, a rich higher order structural diversity depends on the atomic constitution of the precursor molecules, analogous to the dependence of protein folding upon primary structure<sup>51</sup> and of cell membrane function upon surfactant chain length.<sup>51b</sup>

Films containing buried organic interfaces and competing stabilizing interactions are also important as analogues of lipid-protein arrays<sup>52a-b</sup> and covalently bonded lipid-linked proteins.<sup>52c-e</sup> Lipoproteins and lipid-linked proteins are known to interact with cell membranes to cause local disturbances in surfactant packing,<sup>52f</sup> providing the basis for diverse events such as the anchoring of viral coat proteins<sup>52c</sup> and modulation of membrane permeability by oligopeptide drugs.<sup>52g</sup> Further development of the films reported here could provide the basis for modeling such biological processes.

The significance of the observed variable alkyl threshold to the design of new heterostructured assemblies must not be underestimated. The general principle may apply to any system in which sublayers with different lateral interactions are to be incorporated. For example, in Langmuir-Blodgett films<sup>53</sup> or self-assembled multilayers,<sup>4</sup> a rigid sublayer may influence the

assembly process of an adjacent stratum, causing lattice perturbations that would affect the order or disorder of the overall assembly or subsequently assembled strata. Such effects may not be limited to two-dimensional ordering processes and may be important in the design of ordered heterostructured bulk materials.<sup>54</sup> We are presently investigating the thermal and solvent stability of these SAMs, as a quantitative understanding of these subtle inter- and intramolecular interactions is the basis for predicting structure and function in future systems.

## Conclusions

In the series of alkanethiol SAMs  $C_n$ -1AT/Au ( $n = 9, 11-16, 18$ ) containing a single internal amide group, the interaction of a hydrocarbon overlayer with an adjacent amide underlayer has been probed. Variation of the hydrocarbon overlayer thickness allows an understanding of the influence of alkyl chain length on supramolecular structure. FTIR-ERS, supported by electrochemical studies, contact angle goniometry, and XPS, shows that the amide underlayers are identical among the entire series. However, the alkyl overlayers are ordered only above  $n \geq 15$ , indicating that hydrophobic interactions are of secondary importance to hydrogen bonding in establishing film order and stability. The destabilization of alkyl chains adjacent to an amide underlayer (compared to *n*-alkanethiols) is probably due to differences in spacing of the templating head groups. Similarly, the amide underlayer dominates in determining SAM structure most likely because hydrogen bonding interactions are significantly stronger than (1) the hydrophobic interactions they replace and (2) the difference between accessible sulfur-substrate binding modes with which they compete.

This system provides unique opportunities to study the nature of buried organic interfaces. The one-amide amide-alkyl interface behaves in a rigid-elastic manner, similar to a recently proposed model<sup>45b</sup> of interplay between gold-sulfur templating and hydrophobic interactions in *n*-alkanethiol SAMs. This class of SAMs is relevant to diverse areas of research including studies of interactions between lipid-linked peptides and lipid bilayers, control of bulk properties using intermolecular interactions and design of heterostructured monolayers, multilayers and bulk materials.

**Acknowledgment.** This research was supported by the National Science Foundation (NMR: CHE-9421182; XPS: CHE-9512185), the National Science Foundation CAREER Program (CHE-9702726), the Camille and Henry Dreyfus Foundation, the Oregon Medical Research Foundation, and the University Club Foundation of Portland, OR. We thank Kevin Becraft for technical assistance with the electrochemical experiments and Scott M. Reed and Rachel K. Smith for critical readings of the manuscript.

JA9901011

(51) (a) Kelly, J. W. *Structure* **1997**, *5*, 595-600. (b) Yeagle, P. L. *The Structure of Biological Membranes*; CRC: Boca Raton, FL, 1991; pp 539-602, 721-780.

(52) (a) Kaiser, E. T.; Kézdy, F. J. *Annu. Rev. Biophys. Biophys. Chem.* **1987**, *16*, 561-581. (b) von Heijne, G. *Biochim. Biophys. Acta* **1988**, *947*, 307-333. (c) Sefton, B. M.; Buss, J. E. *J. Cell. Biol.* **1987**, *104*, 1449-1453. (d) Yu, Y.-C.; Tirrell, M.; Fields, G. B. *J. Am. Chem. Soc.* **1998**, *120*, 9979-9987. (e) Yu, Y.-C.; Berndt, P.; Tirrell, M.; Fields, G. B. *J. Am. Chem. Soc.* **1996**, *118*, 12515-12520. (f) Batenburg, A. M.; Hibbeln, J. C. L.; de Kruijff, B. *Biochim. Biophys. Acta* **1987**, *903*, 155-165. (g) Surewicz, W. K.; Hantsch, H. H.; Stahl, G. L.; Epand, R. M. *Proc. Natl. Acad. Sci. U.S.A.* **1987**, *84*, 7028-2030.

(53) Maoz, R.; Yam, R.; Berkovic, G.; Sagiv, J. *Thin Films* **1995**, *20*, 41-68.

(54) Krejchi, M. T.; Atkins, E. D. T.; Waddon, A. J.; Fournier, M. J.; Mason, T. L.; Tirrell, D. A. *Science* **1994**, *265*, 1427-1432.